

Effect of Polarimetric Noise on the Estimation of Twist and Magnetic Energy of Force-Free Fields

Sanjiv Kumar Tiwari, P. Venkatakrishnan, Sanjay Gosain and Jayant Joshi

Udaipur Solar Observatory, Physical Research Laboratory,

Dewali, Bari Road, Udaipur-313 001, India

stiwari@prl.res.in

pvk@prl.res.in

sgosain@prl.res.in

jayant@prl.res.in

Received _____; accepted _____

ABSTRACT

The force-free parameter α , also known as helicity parameter or twist parameter, bears the same sign as the magnetic helicity under some restrictive conditions. The single global value of α for a whole active region gives the degree of twist per unit axial length. We investigate the effect of polarimetric noise on the calculation of global α value and magnetic energy of an analytical bipole. The analytical bipole has been generated using the force-free field approximation with a known value of constant α and magnetic energy. The magnetic parameters obtained from the analytical bipole are used to generate Stokes profiles from the Unno-Rachkovsky solutions for polarized radiative transfer equations. Then we add random noise of the order of 10^{-3} of the continuum intensity (I_c) in these profiles to simulate the real profiles obtained by modern spectropolarimeters like Hinode (SOT/SP), SVM (USO), ASP, DLSP, POLIS, SOLIS etc. These noisy profiles are then inverted using a Milne-Eddington inversion code to retrieve the magnetic parameters. Hundred realizations of this process of adding random noise and polarimetric inversion is repeated to study the distribution of error in global α and magnetic energy values. The results show that : (1). the sign of α is not influenced by polarimetric noise and very accurate values of global twist can be calculated, and (2). accurate estimation of magnetic energy with uncertainty as low as 0.5% is possible under the force-free condition.

Subject headings: Sun: magnetic fields, Sun: photosphere

1. Introduction

Helical structures in the solar features like sunspot whirls were reported long back by George E. Hale in 1925 (Hale 1925, 1927). He found that about 80% of the sunspot whirls were counterclockwise in the northern hemisphere and clockwise in the southern hemisphere. Later, in 1941 the result was confirmed by Richardson (Richardson 1941) by extending the investigation over four solar cycles. This hemispheric pattern was found to be independent of the solar cycle. Since the 90's, the subject has been rejuvenated and this hemispheric behaviour independent of sunspot cycle is claimed to be observed for many of the solar features like active regions (Seehafer 1990; Pevtsov et al. 1995; Longcope et al. 1998; Abramenko et al. 1996; Bao & Zhang 1998; Hagino & Sakurai 2005), filaments (Martin et al. 1994; Pevtsov et al. 2003; Bernasconi et al. 2005), coronal loops (Rust & Kumar 1996; Pevtsov & Longcope 2001), interplanetary magnetic clouds (IMCs) (Rust 1994), coronal X-ray arcades (Martin & McAllister 1996) and network magnetic fields (Pevtsov et al. 2001; Pevtsov & Longcope 2007) etc.

Helicity is a physical quantity that measures the degree of linkages and twistedness in the field lines (Berger & Field 1984). Magnetic helicity H_m is given by a volume integral over the scalar product of the magnetic field \mathbf{B} and its vector potential \mathbf{A} (Elsasser 1956).

$$H_m = \int_V \mathbf{A} \cdot \mathbf{B} dV \quad (1)$$

with $\mathbf{B} = \nabla \times \mathbf{A}$.

It is well known that the vector potential \mathbf{A} is not unique, thereby preventing the calculation of a unique value for the magnetic helicity from the equation (1). Seehafer (1990) pointed out that the helicity of magnetic field can best be characterized by the force-free parameter α , also known as the helicity parameter or twist parameter. The

force-free condition (Chandrasekhar 1961; Parker 1979) is given as,

$$\nabla \times \mathbf{B} = \alpha \mathbf{B} \quad (2)$$

Alpha is a measure of degree of twist per unit axial length (see Appendix-A for details of physical meaning of alpha). This is a local parameter which can vary across the field but is constant along the field lines.

Researchers have claimed to have determined the sign of magnetic helicity on the photosphere by calculating alpha, e.g. α_{best} (Pevtsov et al. 1995), averaged alpha e.g. $\langle \alpha_z \rangle = \langle J_z/B_z \rangle$ (Pevtsov et al. 1994) with current density $J_z = (\nabla \times \mathbf{B})_z$. Some authors have used current helicity density $H_c = B_z \cdot J_z$ and α_{av} (Bao & Zhang 1998; Hagino & Sakurai 2004, 2005). A good correlation was found between α_{best} and $\langle \alpha_z \rangle$ by Burnette et al. (2004) and Leka et al. (1996). But the sign of magnetic helicity cannot be inferred from the force-free parameter α under all conditions (See Appendix B).

It is well known that the reliable measurements of vector magnetic fields are needed to study various important parameters like electric currents in the active regions, magnetic energy dissipation during flares, field geometry of sunspots, magnetic twist etc. The study of error propagation from polarization measurements to vector field parameters is very important (Lites & Skumanich 1985; Klimchuk et al. 1992). Klimchuk et al. (1992) have studied the effects of realistic errors e.g., due to random polarization noise, crosstalk between different polarization signals, systematic polarization bias and seeing induced crosstalk etc. on known magnetic fields. They derived analytical expressions for how these errors produce errors in the estimation of magnetic energy (calculated from virial theorem). However, they simulated these effects for magnetographs which sample polarization at few fixed wavelength positions in line wings. It is well known that such observations lead to systematic under-estimation of field strength and also suffer from magneto-optical effects (West & Hagyard 1983). Whereas in our analysis, we simulate the effect of polarimetric

noise on field parameters as deduced by full Stokes inversion. The details are discussed in the section 6.

Pevtsov et al. (1995) found large variations in the global α values from repeated observations of the same active regions. It is important to model the measurement uncertainties before looking for physical explanations for such a scatter.

In a study by Hagyard & Pevtsov (1999) the noise levels in the observed fields were analyzed, but a quantitative relationship between the uncertainties in fields and the uncertainties in global α value were not established. They could only determine the extent to which the incremental introduction of noise affects the observed value of alpha. However, for the proper tracking of error propagation, we need to start with ideal data devoid of noise and with known values of α and magnetic energy. We follow the latter approach in our present analysis.

Here, we estimate the accuracy in the calculation of the α parameter and the magnetic energy due to different noise levels in the spectro-polarimetric profiles. Modern instruments measure the full Stokes polarization parameters within the line profile. Basically there are two types of spectro-polarimeters : (i) Spectrograph based e.g., Advanced Stokes Polarimeter (ASP : Elmore et al. (1992)), Zurich Imaging Polarimeter (ZIMPOL : Keller et al. (1992); Povel (1995); Stenflo (1996); Stenflo & Keller (1997)), THEMIS-MTR (Arnaud et al. (1998)), SOLIS - Vector Spectro-Magnetograph (VSM : Jones et al. (2002); Keller et al. (2003)), Polarimetric Littrow Spectrograph (POLIS : Schmidt et al. (2003)), Diffraction Limited Spectro-polarimeter (DLSP : Sankarasubramanian et al. (2004, 2006)), Hinode (SOT/SP : Tsuneta et al. (2008)), etc. and (ii) Filter-based e.g., Imaging Vector Magnetograph (IVM) at Mees Solar Observatory, Hawaii (Mickey et al. 1996), Solar Vector Magnetograph at Udaipur Solar Observatory (SVM-USO)(Gosain et al. 2004, 2006) etc.

Earlier magnetographs like Crimea (Stepanov & Severny 1962), MSFC (Hagyard et al.

1982), HSP (Mickey 1985), OAO (Makita et al. 1985), HSOS (Ai & Hu 1986), Potsdam vector magnetograph (Staude et al. 1991), SFT (Sakurai et al. 1995) etc. were mostly based on polarization measurements at a few wavelength positions in the line wings and hence subject to Zeeman saturation effects as well as magneto-optical effects like Faraday rotation (West & Hagyard 1983; Hagyard et al. 2000).

The magnetic field vector deduced from Stokes profiles by modern techniques are almost free from such effects (Skumanich & Lites 1987; S’anchez Almeida 1998; Socas-Navarro 2001).

This paper serves three purposes. First, we estimate the error in the calculation of field strength, inclination and azimuth and thereafter in the calculation of the vector field components B_x , B_y and B_z . Second, we estimate the error in the determination of global α due to noise in polarimetric profiles constructed from the analytical vector field data. Third, we estimate the error in the calculation of magnetic energy derived using virial theorem, due to polarimetric noise.

In the next section (section 2) we discuss a direct method for calculation of a single global α for an active region. In section 3, we describe the method of simulating an analytical bipole field. Section 4 contains the analysis and the results. Error estimation in global α is given in section 5. In section 6 we discuss the process of estimating the error in the virial magnetic energy. Section 7 deals with discussion and conclusions.

2. A direct method for calculation of global α

Taking the z-component of magnetic field, from the force-free field equation (2) α can be written as,

$$\alpha = \frac{(\nabla \times \mathbf{B})_z}{B_z} \quad (3)$$

For a least squares minimization, we should have

$$\begin{aligned} \sum (\alpha - \alpha_g)^2 &= \text{minimum} \\ \text{or,} \quad \alpha_g &= (1/N) \sum \alpha \end{aligned} \quad (4)$$

where α is the local value at each pixel, α_g is the global value of α for the complete active region and N is total number of pixels.

Since eqn.(4) will lead to singularities at the neutral lines where B_z approaches 0, therefore the next moment of minimization,

$$\sum (\alpha - \alpha_g)^2 B_z^2 = \text{minimum} \quad (5)$$

should be used. From eqn.(5) we have

$$\frac{\partial}{\partial \alpha_g} (\sum (\alpha - \alpha_g)^2 B_z^2) = 0 \quad (6)$$

which leads to the following result,

$$\alpha_g = \frac{\sum (\frac{\partial B_y}{\partial x} - \frac{\partial B_x}{\partial y}) B_z}{\sum B_z^2} \quad (7)$$

This formula gives a single global value of α in a sunspot and is the same as $\alpha_{av}^{(2)}$ of Hagino & Sakurai (2004). We prefer this direct way of obtaining global α which is different from the method discussed in Pevtsov et al. (1995) for determining α_{best} . The main differences are : (1). the singularities at neutral line are automatically avoided in our method by using the second moment of minimization and (2). the computation of constant α force-free fields for different test values of α is not required. Hagino & Sakurai (2004) used a different parameter $\alpha_{av}^{(1)}$ to avoid the effect of Faraday rotation in sunspot umbrae. However, modern inversion techniques using complete Stokes profiles are free of this problem.

It must be noted that one can generate different values of α_g using higher moments of minimization, e.g., by weighting J_z with B_z^n , with $n=3, 5, 7, \dots$ etc. The higher moments

will be more sensitive to spatial variation of B_z . Such large and complex variation of B_z is found generally in flare productive active regions (Ambastha et al. 1993; Wang et al. 1996; Hagyard et al. 1999). Thus we can try to use higher order α_g as a global index for predicting the flare productivity in active regions.

Finally, to compute α_g we need all the three components of magnetic field which is obtained from the measurements of vector magnetograms. However, here we use the analytically generated bipole, as discussed in the following section, with known values of all the magnetic parameters to investigate the effect of polarimetric noise.

3. Generation of theoretical bipole

We use the analytic, non-potential force-free fields of the form derived by Low (1982). These fields describe an isolated bipolar magnetic region which is obtained by introducing currents into a potential field structure. This potential field is produced by an infinite straight line current running along the intersection of the planes $y = 0$ and $z = -a$, where negative sign denotes planes below the photosphere $z = 0$. At the photosphere ($z = 0$), the field has the following form :

$$B_x = -\frac{B_0 a}{r} \cos \phi(r) \quad (8)$$

$$B_y = \frac{B_0 a x y}{r(y^2 + a^2)} \cos \phi(r) - \frac{B_0 a^2}{(y^2 + a^2)} \sin \phi(r) \quad (9)$$

$$B_z = \frac{B_0 a^2 x}{r(y^2 + a^2)} \cos \phi(r) - \frac{B_0 a y}{(y^2 + a^2)} \sin \phi(r) \quad (10)$$

where B_0 is the magnitude of the field at origin and $r^2 = x^2 + y^2 + a^2$. The function $\phi(r)$ is a free generating function related to the force-free parameter α (see eqn (2)) by

$$\alpha = -\frac{d\phi}{dr} \quad (11)$$

which determines the current structure and hence the amount and location of shear present in the region. By choosing $\phi(r) = \text{constant} = \pi/2$ we can obtain a simple potential (current-free, $\alpha = 0$) field produced by the infinite line current lying outside the domain. Steeper gradient of $\phi(r)$ results in a more sheared (non-potential) field.

In equation (11) the sign on the right hand side is taken positive in the paper by Low (1982) which is a typing mistake (confirmed by B. C. Low, private communication). We mention this here to avoid carrying forward of this typo as was done in Wilkinson et al. (1989).

A grid of 100 x 100 pixels was selected for calculating the field components. The magnitude of field strength at origin has been taken as 1000G and the value of ‘a’ is taken as 15 pixels (below the photosphere, $z = 0$).

The simulated field components with corresponding contours are shown in the figure 1.

Here we use the following function (e.g., Wilkinson et al. (1989)) for the generation of the field components (B_x, B_y, B_z) :

$$\phi(r) = \frac{\pi r - a}{2 \cdot 2a}, \quad r \leq 3a \quad (12)$$

$$= \frac{\pi}{2}, \quad r > 3a \quad (13)$$

Results for the fields generated by different $\phi(r)$ are quantitatively similar. In this way we generate a set of vector fields with known values of α .

Most of the time one of the bipoles of a sunspot observed on the Sun is compact (leading) and the other (following) is comparatively diffuse. Observations of compact pole gives half of the total flux of the sunspot and is mostly used for analysis. One can derive the twist present in the sunspot using one compact pole of the bipolar sunspot for constant α . Thus we have selected a single polarity of the analytical bipole as shown in figure 1 to calculate the twist.

Fine structure in real sunspots is difficult to model. Our analysis applies to the large scale patterns of the magnetic field regardless of fine structure.

All the following sections discuss the analysis and results obtained.

4. Profile generation from the analytical data and inversion

Using the analytical bipole method (Low 1982) the non-potential force-free field components B_x , B_y & B_z in a plane have been generated and are given as in equations (8), (9) & (10). We have shown B_x , B_y , & B_z maps (generated on a grid of 100 x 100 pixels) in figure 1. From these components we have derived magnetic field strength (B), inclination (γ) and azimuth (ξ : free from 180° ambiguity). In order to simulate the effect of typical polarimetric noise in actual solar observations on magnetic field measurements and study the error in the calculation of α and magnetic energy, we have generated the synthetic Stokes profiles for each B , γ and ξ in a grid of 100 x 100 pixels, using the He-Line Information Extractor “HELIX” code (Lagg et al. 2004). This code is a Stokes inversion code based on fitting the observed Stokes profiles with synthetic ones obtained by Unno-Rachkovsky solutions (Unno 1956; Rachkovsky 1967) to the polarized radiative transfer equations (RTE) under the assumption of Milne-Eddington (ME) atmosphere (Landolfi & Landi Degl’Innocenti 1982) and local thermodynamical equilibrium (LTE). However, one can also use this code for generating synthetic Stokes profiles for an input model atmosphere. The synthetic profiles are functions of magnetic field strength (B), inclination (γ), azimuth (ξ), line of sight velocity (v_{Los}), Doppler width (v_{Dopp}), damping constant (Γ), ratio of the center to continuum opacity (η_0), slope of the source function (S_{grad}) and the source function (S_0) at $\tau = 0$. The filling factor is taken as unity. In our profile synthesis only magnetic field parameters B , γ , ξ are varied while other model parameters are kept same for all pixels. The typical values of other thermodynamical

parameters are given in table 1. We use the same parameters for all pixels. Further, all the physical parameters at each pixel are taken to be constant in the line forming region. However, one must remember that real solar observations have often Stokes V area asymmetries (Solanki 1989; Khomenko et al. 2005) as a result of vertical magnetic and velocity field gradients present in the line forming region. This has not been taken into account in our simulations.

A set of Stokes profiles with 0.5% and 2.0% noise for a pixel is shown in figure 2.

The wavelength grid used for generating synthetic spectral profiles is same as that of Hinode (SOT/SP) data which are as follows : start wavelength of 6300.89 Å, spectral sampling 21.5 mÅ/pixel, and 112 spectral samples. We add normally distributed random noise of different levels in the synthetic Stokes profiles. Typical noise levels in Stokes profiles obtained by Hinode (SOT/SP) normal mode scan are of the order of 10^{-3} of the continuum intensity, I_c (Ichimoto et al. 2008). We add random noise of 0.5 % of the continuum intensity I_c to the polarimetric profiles. In addition, we also study the effect of adding a noise of 2.0% level to Stokes profiles as a worst case scenario. We add 100 realizations of the noise of the orders mentioned above to each pixel and invert the corresponding 100 noisy profiles using the “HELIX” code.

The guess parameters to initialize the inversion are generated by perturbing known values of B , γ and ξ by 10%. Thus after inverting 100 times we get 100 sets of B , γ & ξ maps for the input B , γ & ξ values from bipole data. In this way we estimate the spread in the derived field values for various field strengths, inclinations etc. First, the inversion is done without adding any noise in the profiles to check the accuracy of inversion process. We get the results retrieved in this process which are very similar to that of the initial analytical ones. The scatter plot of input field strength, inclination, azimuth against the corresponding retrieved strength, inclination, azimuth after noise addition and inversion is

shown in figure 3 (upper panel). Typical B_x , B_y & B_z maps with different noise levels are shown in the lower panel. As the noise increases B_x , B_y & B_z maps become more grainy.

From the plots shown in figure 3 we can see that the error in the field strength for a given noise level decreases for strong fields. This is similar to results of Venkatakrisnan & Gary (1989). As the noise increases in the profiles, error in deriving the field strength increases. We find that the error in the field strength determination is $\sim 15\%$ for 0.5% noise and $\sim 25\%$ for 2% noise in the profiles. Inclination shows more noise near 0° & 180° than at $\sim 90^\circ$. The error is less even for large noisy profiles for the inclination angles between $\sim 50^\circ - 130^\circ$. The reason for this may be understood in the following way. Linear polarization is weaker near 0 and 180° inclinations and is therefore more affected by the noise. The azimuth determination has inherent 180° ambiguity due to insensitivity of Zeeman effect to orientation of transverse fields. Thus in order to compare the input and output azimuths we resolve this ambiguity in ξ_{out} by comparing it with ξ_{in} i.e., the value of ξ_{out} which makes acute angle with ξ_{in} has been taken as correct. We can see azimuth values after resolving the ambiguity in this way show good correlation with input azimuth values. Some scatter is due to the points where ambiguity was not resolved due to 90° difference in ξ_{in} and ξ_{out} .

First, the α_g was calculated from the vector field components derived from the noise free profiles to verify the method of calculating global alpha and also the inversion process. We have used the single polarity to calculate global alpha present in sunspot as discussed in section 3. We retrieved the same value of α_g as calculated using the initial analytical field components. From the figure 4. we can see that the effect of noise on the field components is not much for the case of 0.5% noise but as the noise in the profiles is increased to 2.0% , the field components specially transverse fields show more uncertainty. The vertical field is comparatively less affected with noise. The scatter plot in figure 4. shows that the inversion

gives good correlation to the actual field values. The points with large scatter are due to poor “signal to noise” ratio in the simulated profiles. The mean percentage error in the further discussions is given in terms of weighted average of error.

5. Estimation of the error in the calculation of global alpha (α_g)

We calculate the percentage error in global alpha each time after getting the inverted results, for both the cases when 0.5% and 2.0% (of I_c) noise is added in the profiles, by the following relation :

$$\frac{\Delta\alpha_g}{\alpha_g}(\%) = \frac{\alpha_g^* - \alpha_g}{\alpha_g} \times 100 \quad (14)$$

where α_g^* is calculated global alpha and α_g is the analytical global alpha.

The histogram of the results obtained is shown in figure 5.

First, we inverted the profiles without adding any noise and calculated α_g from retrieved results to compare it with the ‘true’ α_g calculated from the analytically generated vector field components. We get less than 0.002% difference in the both α_g values.

For the case of 0.5% noise in polarimetric profiles we get a mean error of 0.3% in the calculation of α_g and error is never more than 1%. Thus the calculation of α_g is almost free from the effect of noise in this case. Hence, by using data from Hinode (SOT/SP), one can derive the accurate value of twist present in a sunspot.

If 2.0% noise is present in the polarization, then maximum $\sim 5\%$ error is obtained. Weighted average shows only 1% error. Thus the estimation of alpha is not influenced very much even from the data obtained with old and ground based magnetographs. In any event it is unlikely that a realistic error will be large enough to create a change in the sign of α_g .

6. Estimation of the error in the calculation of magnetic energy (E_m)

The magnetic energy has been calculated using virial theorem. One form of the general virial theorem (Chandrasekhar 1961) states that for a force-free magnetic field, the magnetic energy contained in a volume V is given by a surface integral over the boundary surface S ,

$$\int \frac{1}{8\pi} B^2 dV = \frac{1}{4\pi} \int \left[\frac{1}{2} B^2 \mathbf{r} - (\mathbf{B} \cdot \mathbf{r}) \mathbf{B} \right] \cdot \hat{\mathbf{n}} dS \quad (15)$$

where \mathbf{r} is the position vector relative to an arbitrary origin, and $\hat{\mathbf{n}}$ is the normal vector at surface. Let us adopt Cartesian coordinates, taking as $z=0$ plane for photosphere. This assumption is reasonable because the size of sunspots are very small compared to the radius of the Sun. If we make the further reasonable assumption that the magnetic field strength decreases with distance more rapidly than $r^{-3/2}$ whereas a point dipole field falls off as r^{-3} , then the equation (15) can be simplified to (Molodensky 1974)

$$\int \frac{1}{8\pi} B^2 dx dy dz = \frac{1}{4\pi} \int (x B_x + y B_y) B_z dx dy \quad (16)$$

where x and y are the horizontal spatial coordinates. B_x , B_y & B_z are the vector magnetic field components. This equation (16) is referred as the “magnetic virial theorem”.

Thus magnetic energy of an active region can be calculated simply by substituting the derived vector field components into the surface integral of equation (16) (Low 1982, 1985, 1989). Magnetic field should be solenoidal and force-free as is the case for our analytical field. So the energy integral is independent of choice of the origin.

If all the above conditions are satisfied then the remaining source of uncertainty in the magnetic energy estimation is the errors in the vector field measurements themselves. So, before the virial theorem can be meaningfully applied to the Sun, it is necessary first to understand how the errors in the vector field measurements produce errors in the calculated magnetic energies.

Earlier, the efforts were made to estimate the errors (Gary et al. 1987; Klimchuk et al. 1992) for magnetographs like Marshall Space Flight Center (MSFC) magnetograph. Gary et al. (1987) constructed a potential field from MSFC data and computed its virial magnetic energy. Then, they modified the vector field components by introducing random errors in B_x , B_y and B_z and recomputed the energy. They found the two energies differ by 11%. Klimchuk et al. (1992) approached the problem differently. They introduced errors in the polarization measurements from which the field is derived instead of introducing errors to magnetic fields directly. In this way they were able to approximate reality, more closely and were able to include certain type of errors such as crosstalk which were beyond the scope of the treatment by Gary et al. (1987). They found that the energy uncertainties are likely to exceed 20% for the observations made with the vector magnetographs present at that time (e.g. MSFC).

Here, our approach is very similar to that of Klimchuk et al. (1992) except that we consider full Stokes profile measurements to derive the magnetic fields like in the most of the recent vector magnetographs e.g., Hinode (SOT/SP), SVM-USO etc. as mentioned earlier. We begin with an analytical field, determine polarization signal as explained in earlier parts, introduce the random noise of certain known levels (0.5% & 2.0% of I_c) in the polarization profiles, infer an ‘observed’ magnetic field after doing the inversion of the noisy profiles, compute an ‘observed’ magnetic energy from the ‘observed’ field and then compare this energy with the energy of the ‘true’ magnetic field. The percentage error is calculated from the following expression:

$$\frac{\Delta E_m}{E_m}(\%) = \frac{E_m^* - E_m}{E_m} \times 100 \quad (17)$$

where E_m^* is ‘observed’ energy and E_m is ‘true’ energy. All the above processes have been described in detail in section 4.

Figure 6 shows the uncertainty estimated in the calculation of magnetic energy in two

cases when error in the polarimetric profiles is 0.5% and 2.0% of I_c . Needless to say, we first checked the procedure by calculating the magnetic energy from the vector fields derived from inverted results with no noise in the profiles. We found the same energy as calculated from the initial analytical fields.

We can see that the magnetic energy can be calculated with a very good accuracy when less noise is present in the polarization as is observed in the modern telescopes like Hinode (SOT/SP) for which very small (of the order of 10^{-3} of I_c) noise is expected in profiles. We find that a mean of 0.5% and maximum up to 2% error is possible in the calculation of magnetic energy with such data. So, the magnetic energy calculated from the Hinode data will be very accurate provided the force-free field condition is satisfied.

The error in the determination of magnetic energy increases for larger levels of noise. In the case of high noise in profiles (e.g. 2.0% of I_c) the energy estimation is very much vulnerable to the inaccuracies of the field values. We replaced the inverted value of the field parameters with the analytical value wherever the inverted values deviated by more than 50% of the ‘true’ values. We then get the result shown in the right panel. We can see that the error is very small even in this case. The mean value of error is $\sim 0.7\%$.

7. Discussion and Conclusions

We have discussed the direct method of estimating α_g from vector magnetograms using the 2^{nd} moment of minimization. The higher order moments also hold promise for generating an index for predicting the flare productivity in active regions.

The global value of twist of an active region can be measured with a very good accuracy by calculating α_g . Accurate value of twist can be obtained even if one polarity of a bipole is observed.

The magnetic energy calculation is very accurate as seen from our results. Very less error (approximately 0.5%) is seen in magnetic energy with 0.5% noise in the profiles. Thus we conclude that the magnetic energy can be estimated with very good accuracy using the data obtained from modern telescopes like Hinode (SOT/SP). This gives us the means to look for magnetic energy changes released in weak C-class flares which release radiant energy of the order of 10^{30} ergs (see Appendix-C), thereby improving the statistics.

These energy estimates are however subject to the condition that the photospheric magnetic field is force-free, a condition which is not always met with. We must then obtain the energy estimates using vector magnetograms observed at higher atmospheric layers where the magnetic field is force-free (Metcalf et al. 1995).

The 180° azimuthal ambiguity (AA) is another source of error for determining parameters like α_g and magnetic free energy in real sunspot observations. The smaller the polarimetric noise, the smaller is the uncertainty in azimuth determination, thereby allowing us to extend the range of the acute angle method used in our analysis. On the other hand it is difficult to predict the level of uncertainty produced by AA. Influence of AA is felt more at highly sheared regions which will anyway deviate from the global alpha value. Thus, avoiding such pixels will improve determination of α_g . Magnetic energy calculation at such pixels could be done by comparing energy estimates obtained by ‘flipping’ the azimuths and choosing the mean of the smallest and the largest estimate of the energy. Here we assume that half the number of pixels have the true azimuth. This is the best one can do for a problem that really has no theoretical solution allowed by the Zeeman effect (but see also, Metcalf et al. (2006) and references therein). Observational techniques such as use of chromospheric chirality (López Ariste et al. 2006; Martin et al. 2008; Tiwari et al. 2008) or use of magnetograms observed from different viewing angles could perhaps resolve the AA .

Patches of both signs of alpha can be present in a single sunspot (Pevtsov et al. 1994;

Hagino & Sakurai 2004). In those cases the physical meaning of α_g becomes unclear. Efforts are needed to understand the origin of such complex variation of α in a sunspot. Real sunspots show filamentary structures. If this structure is accompanied by local variations of α , then does the global α result from correlations in the local α values? Or, are the small scale variations due to a turbulent cascade from the large scale features? The answers to these questions are beyond the scope of our present study. Modeling sunspots with such complex fine structures is a great challenge. However, we plan to address the question of fine structure of twists in real sunspots observed from HINODE (SOT/SP), in our forthcoming study.

For the present, we demonstrate that the global twist present in an active region can be accurately measured without ambiguity in its sign. Furthermore, the high accuracy of magnetic energy estimation that can be obtained using data from modern instruments will improve the probability for detecting the flare related changes in the magnetic energy of active regions.

Acknowledgments

We thank Professor E. N. Parker for discussion leading to our understanding about the physical meaning of α parameter during his visit to Udaipur Solar Observatory in November 2007. We also thank him for looking at an earlier draft of the manuscript and for making valuable comments to improve it. One of us (Jayant Joshi) acknowledge financial support under ISRO / CAWSES - India programme. We thank Dr. A. Lagg for providing the HELIX code. We are grateful for the valuable suggestions and comments of the referee which have significantly improved the manuscript.

Appendix

A. Physical meaning of force-free parameter α

(Derived from the discussions with Professor Eugene N. Parker during his visit to Udaipur Solar Observatory)

Taking surface integral on both sides of eqn. (2), we get

$$\begin{aligned}\alpha \int dS \cdot \mathbf{B} &= \int dS \cdot \nabla \times \mathbf{B} \\ &= \oint dl \cdot \mathbf{B} \quad (\text{from Stokes theorem})\end{aligned}\tag{A1}$$

or,

$$\alpha = \oint \frac{dl \cdot \mathbf{B}}{\Phi}\tag{A2}$$

In the cylindrical coordinate we can write eqn.(A2) as

$$\begin{aligned}\alpha &= \frac{2\pi\varpi B_\phi}{\pi\varpi^2 B_z} \\ &= \frac{2B_\phi}{\varpi B_z}\end{aligned}\tag{A3}$$

where z and ϖ are axial and radial distances from origin, respectively

The equation of field lines in cylindrical coordinates is given as :

$$\frac{B_z}{dz} = \frac{B_\phi}{\varpi d\phi}\tag{A4}$$

or,

$$\frac{B_\phi}{B_z} = \frac{\varpi d\phi}{dz}\tag{A5}$$

Using eqns. (A3) & (A5), we get

$$\alpha = 2 \frac{d\phi}{dz}\tag{A6}$$

From equation (A6) it is clear that the α gives twice the degree of twist per unit axial length. If we take one complete rotation of flux tube i.e., $\phi = 2\pi$, and loop length $\lambda \approx 10^9 \text{meters}$, then

$$\alpha = \frac{2 \times 2\pi}{\lambda} \tag{A7}$$

comes out of the order of approximately 10^{-8} per meter.

B. Correlation between sign of magnetic helicity and that of α

Eqn. (2) can be written as

$$\begin{aligned} \nabla \times \mathbf{B} &= \alpha(\nabla \times \mathbf{A}) \\ &= \nabla \times (\alpha\mathbf{A}) \end{aligned} \tag{B1}$$

giving vector potential in terms of scalar potential ϕ as

$$\mathbf{A} = \mathbf{B}\alpha^{-1} + \nabla\phi \tag{B2}$$

which is valid only for constant α .

Using this relation in eqn.(1), we get magnetic helicity as

$$\begin{aligned} H_m &= \int (\mathbf{B}\alpha^{-1} + \nabla\phi) \cdot \mathbf{B} \, dV \\ &= \int B^2\alpha^{-1}dV + \int (\mathbf{B} \cdot \nabla)\phi \, dV \end{aligned} \tag{B3}$$

Second term in the right hand side of eqn. (B3) can be written as,

$$\begin{aligned} \int (\mathbf{B} \cdot \nabla)\phi \, dV &= \int \nabla \cdot (\phi\mathbf{B}) \, dV \\ &= \int (\phi \mathbf{B}) \cdot \mathbf{n} \, dS \end{aligned} \tag{B4}$$

(from Gauss Divergence Theorem) which is equal to zero for a closed volume where magnetic field does not cross the volume boundary ($\mathbf{n} \cdot \mathbf{B} = 0$) provided that ϕ remains finite on the surface. Therefore, we get magnetic helicity in terms of α as

$$H_m = \int B^2\alpha^{-1} \, dV \tag{B5}$$

which shows that the force free parameter α has the same sign as that of the magnetic helicity. However, if $\mathbf{n} \cdot \mathbf{B} \neq \mathbf{0}$, then the contribution of the second term in eqn. (B3) remains unspecified. Thus it is not correct to use alpha to determine the sign of magnetic helicity for the half space above the photosphere since $\mathbf{n} \cdot \mathbf{B} \neq \mathbf{0}$ at the photosphere.

C. Estimate of energy release in different classes of X-ray flares:

With the simplifying assumption that all classes of soft X-ray flares have a typical duration of 16 min (Drake 1971), we can see that the energy released in the different classes of flares will be proportional to their peak power. Since X-class flares typically release radiant energy of the order of 10^{32} ergs (Emslie et al. 2005), therefore M-class, C-class, B-class and A-class flares will release radiant energy of the order of respectively 10^{31} , 10^{30} , 10^{29} and 10^{28} ergs.

Table 1. Model parameters for generating synthetic profile

Model Parameter	Value
Doppler velocity, v_{Los} (ms^{-1})	0
Doppler width, v_{Dopp} ($\text{m}\text{\AA}$)	20
Ratio of center to continuum opacity, η_o	20
Source function, S_o	0.001
Slope of the source function, S_{grad}	1.0
Damping constant, Γ	1.4

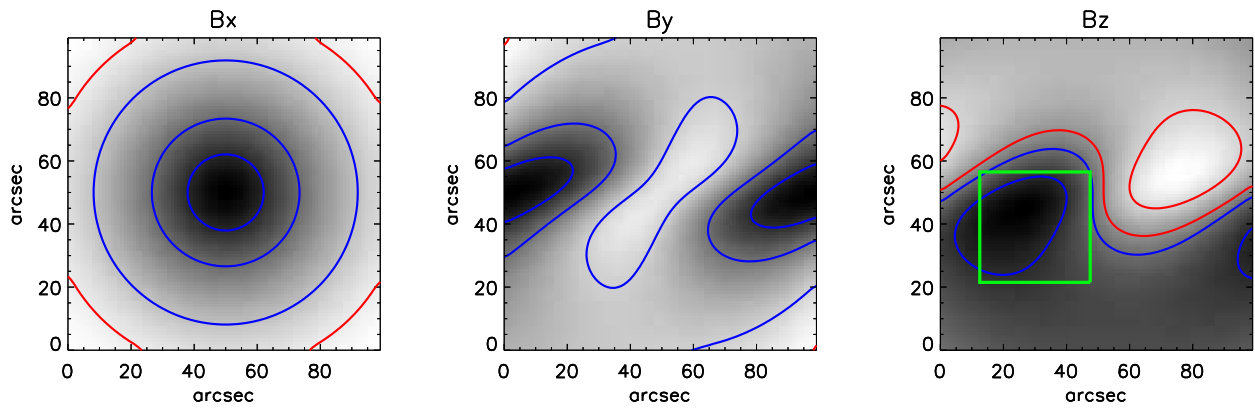


Fig. 1.— Contours of the field components overlaid on their gray-scale images. The contour levels are 100, 500 and 800 G of magnetic fields. The red and blue contours denote the ‘positive’ and ‘negative’ polarities, respectively. The green box in B_z shows the area which is selected for the calculation of global α . For details see the text.

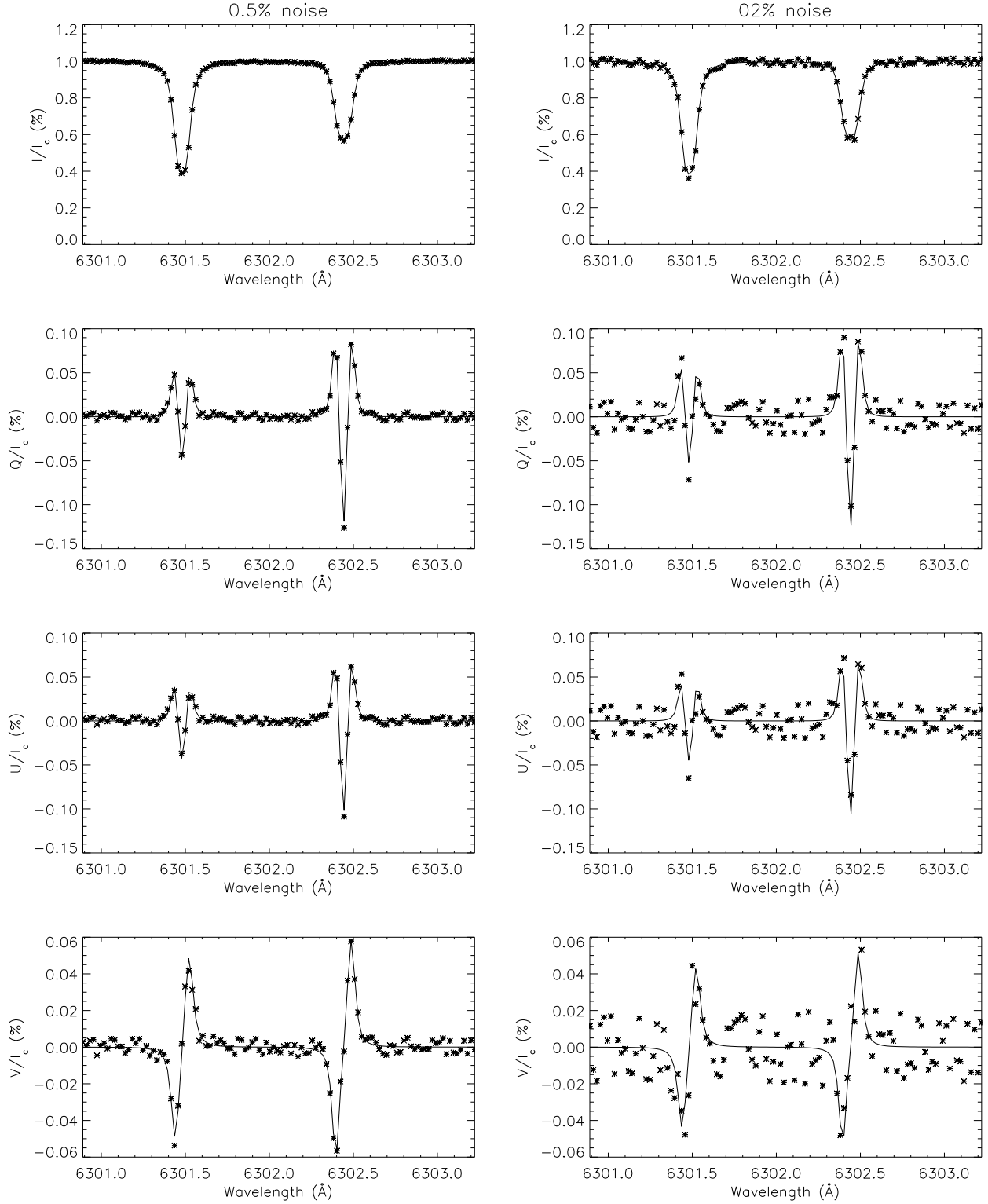


Fig. 2.— Example of Stokes profiles with 0.5% (left column) and 2.0% (right column) noise along with fitted profiles. The input parameters for the associated pixel are as follows : field strength= 861 G, inclination= 101° , azimuth= 19° . The corresponding output parameters are 850 G, 101° , 19° for 0.5% noise and 874 G, 99° , 19° for 2.0% noise.

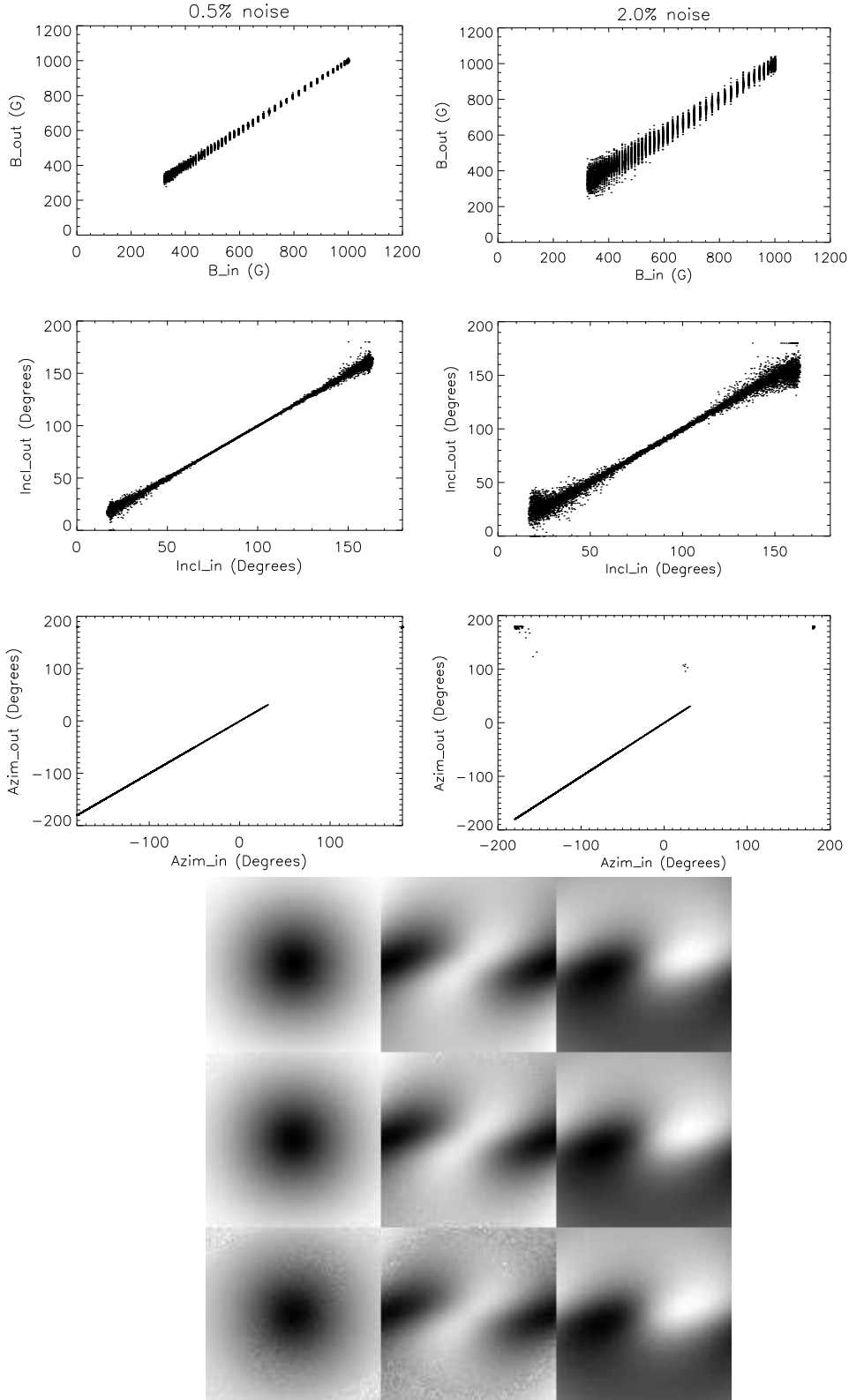


Fig. 3.— Scatter plot (upper panel) between the field strength, inclination and azimuth before and after inversion with 0.5% (1st column) and 2.0% (2nd column) noises in the profiles. The lower panel shows the images of vector fields B_x , B_y & B_z before (1st row) and after

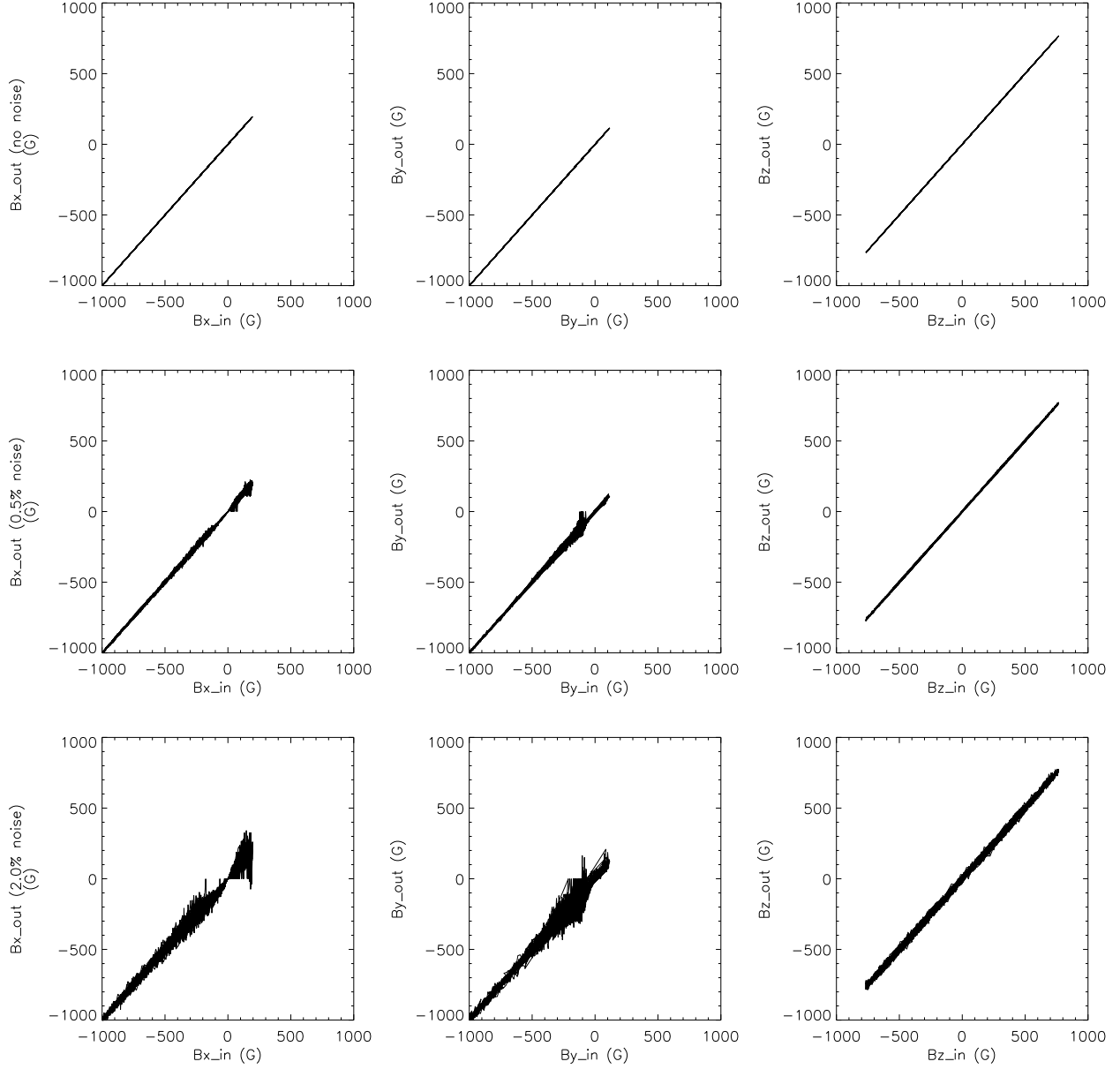


Fig. 4.— Scatter plot between B_x , B_y & B_z before and after inversion without noise (1^{st} row) and with adding noise in the profiles: 2^{nd} row with 0.5% noise and 3^{rd} row with 2.0% noise (of I_c) in the polarimetric profiles.

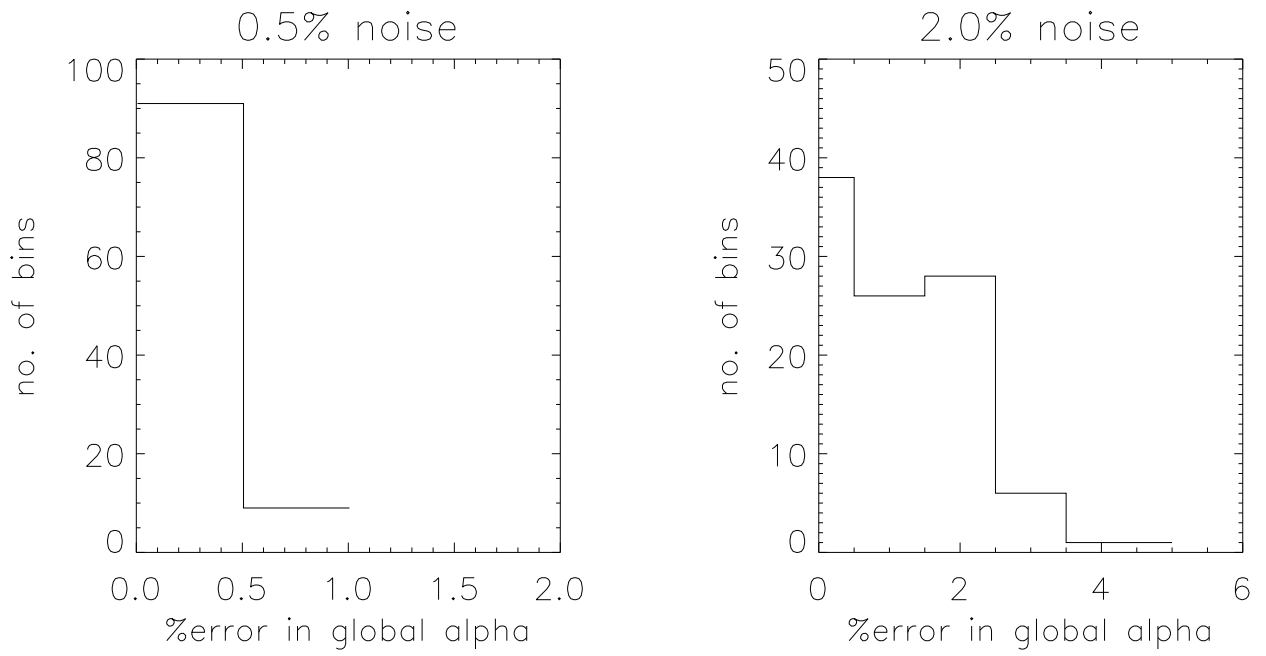


Fig. 5.— Histogram of the percentage error in calculation of α_g with 0.5% and 2.0% noise (of I_c) in polarimetric profiles, respectively.

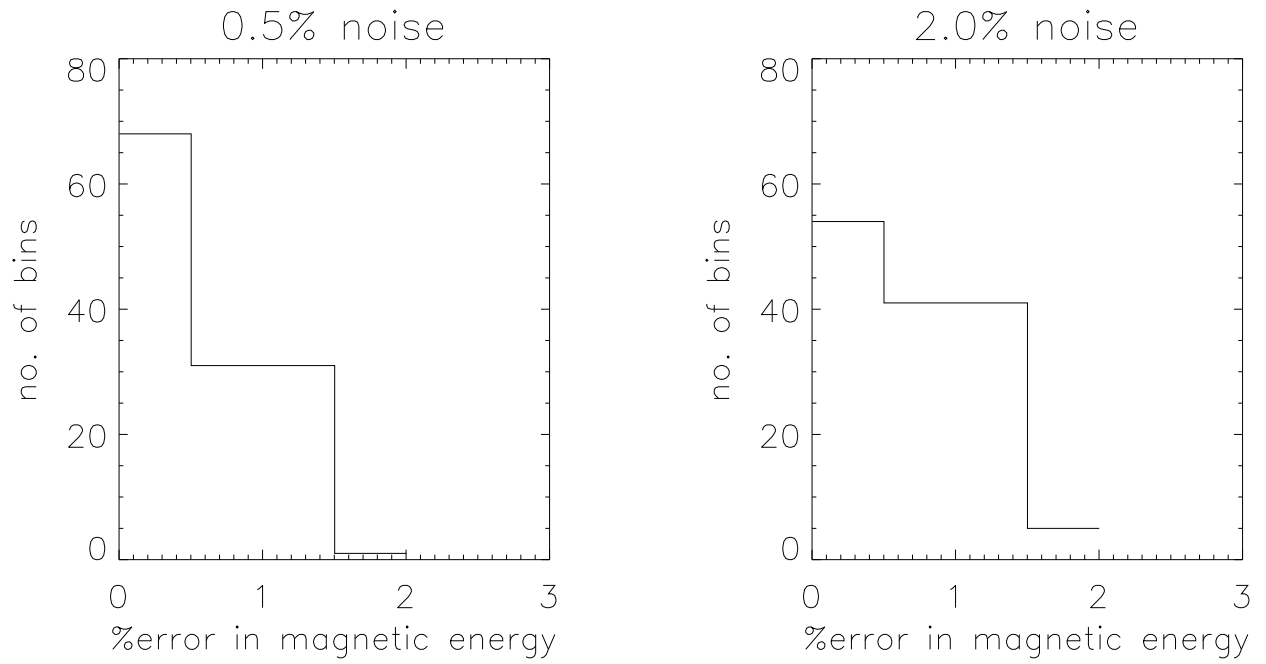


Fig. 6.— Histogram of the percentage error in calculation of magnetic energy when 0.5% and 2.0% noise (of I_c) is present in polarimetric profiles, respectively.

REFERENCES

- Abramenko, V. I., Wang, T., & Yurchishin, V. B. 1996, *Sol. Phys.*, 168, 75
- Ai, G.-X., & Hu, Y.-F. 1986, *Publications of the Beijing Astronomical Observatory*, 8, 1
- Ambastha, A., Hagyard, M. J., & West, E. A. 1993, *Sol. Phys.*, 148, 277
- Arnaud, J., Mein, P., & Rayrole, J. 1998, in *ESA Special Publication*, Vol. 417, *Crossroads for European Solar and Heliospheric Physics. Recent Achievements and Future Mission Possibilities*, 213
- Bao, S., & Zhang, H. 1998, *ApJ*, 496, L43
- Berger, M. A., & Field, G. B. 1984, *Journal of Fluid Mechanics*, 147, 133
- Bernasconi, P. N., Rust, D. M., & Hakim, D. 2005, *Sol. Phys.*, 228, 97
- Burnette, A. B., Canfield, R. C., & Pevtsov, A. A. 2004, *ApJ*, 606, 565
- Chandrasekhar, S. 1961, Chapter-2 : Hydrodynamic and hydromagnetic stability
(International Series of Monographs on Physics, Oxford: Clarendon, 1961)
- Drake, J. F. 1971, *Sol. Phys.*, 16, 152
- Elmore, D. F., et al. 1992, in *Society of Photo-Optical Instrumentation Engineers (SPIE) Conference Series*, Vol. 1746, *Society of Photo-Optical Instrumentation Engineers (SPIE) Conference Series*, ed. D. H. Goldstein & R. A. Chipman, 22
- Elsasser, W. M. 1956, *Rev. Mod. Phys.*, 28, 135
- Emslie, A. G., Dennis, B. R., Holman, G. D., & Hudson, H. S. 2005, *Journal of Geophysical Research (Space Physics)*, 110, 11103
- Gary, G. A., Moore, R. L., Hagyard, M. J., & Haisch, B. M. 1987, *ApJ*, 314, 782

- Gosain, S., Venkatakrishnan, P., & Venugopalan, K. 2004, *Experimental Astronomy*, 18, 31
- Gosain, S., Venkatakrishnan, P., & Venugopalan, K. 2006, *Journal of Astrophysics and Astronomy*, 27, 285
- Hagino, M., & Sakurai, T. 2004, *PASJ*, 56, 831
- Hagino, M., & Sakurai, T. 2005, *PASJ*, 57, 481
- Hagyard, M. J., Adams, M. L., Smith, J. E., & West, E. A. 2000, *Sol. Phys.*, 191, 309
- Hagyard, M. J., Cumings, N. P., West, E. A., & Smith, J. E. 1982, *Sol. Phys.*, 80, 33
- Hagyard, M. J., & Pevtsov, A. A. 1999, *Sol. Phys.*, 189, 25
- Hagyard, M. J., Stark, B. A., & Venkatakrishnan, P. 1999, *solphys*, 184, 133
- Hale, G. E. 1925, *PASP*, 37, 268
- Hale, G. E. 1927, *Nature*, 119, 708
- Ichimoto, K., et al. 2008, *Sol. Phys.*, 249, 233
- Jones, H. P., Harvey, J. W., Henney, C. J., Hill, F., & Keller, C. U. 2002, in *ESA Special Publication, Vol. 505, SOLMAG 2002. Proceedings of the Magnetic Coupling of the Solar Atmosphere Euroconference*, ed. H. Sawaya-Lacoste, 15
- Keller, C. U., Aebersold, F., Egger, U., Povel, H. P., Steiner, P., & Stenflo, J. O. 1992, *LEST Found., Tech. Rep., No. 53*, 53
- Keller, C. U., Harvey, J. W., & Giampapa, M. S. 2003, in *Presented at the Society of Photo-Optical Instrumentation Engineers (SPIE) Conference, Vol. 4853, Society of Photo-Optical Instrumentation Engineers (SPIE) Conference Series*, ed. S. L. Keil & S. V. Avakyan, 194

- Khomenko, E. V., Shelyag, S., Solanki, S. K., & Vögler, A. 2005, *A&A*, 442, 1059
- Klimchuk, J. A., Canfield, R. C., & Rhoads, J. E. 1992, *ApJ*, 385, 327
- Lagg, A., Woch, J., Krupp, N., & Solanki, S. K. 2004, *A&A*, 414, 1109
- Landolfi, M., & Landi Degl’Innocenti, E. 1982, *Sol. Phys.*, 78, 355
- Leka, K. D., Canfield, R. C., McClymont, A. N., & van Driel-Gesztelyi, L. 1996, *ApJ*, 462, 547
- Lites, B. W., & Skumanich, A. 1985, in *Measurements of Solar Vector Magnetic Fields*, ed. M. J. Hagyard, 342
- Longcope, D. W., Fisher, G. H., & Pevtsov, A. A. 1998, *ApJ*, 507, 417
- López Ariste, A., Aulanier, G., Schmieder, B., & Sainz Dalda, A. 2006, *A&A*, 456, 725
- Low, B. C. 1982, *Sol. Phys.*, 77, 43
- Low, B. C. 1985, *Measurements of Solar Vector Magnetic Fields*, 2374, 49
- Low, B. C. 1989, *Washington DC American Geophysical Union Geophysical Monograph Series*, 54, 21
- Makita, M., Hamana, S., Nishi, K., Shimizu, M., & Koyano, H. 1985, *PASJ*, 37, 561
- Martin, S. F., Bilimoria, R., & Tracadas, P. W. 1994, in *Solar Surface Magnetism*, ed. R. J. Rutten & C. J. Schrijver, 303
- Martin, S. F., Lin, Y., & Engvold, O. 2008, *Sol. Phys.*, 250, 31
- Martin, S. F., & McAllister, A. H. 1996, in *IAU Colloq. 153: Magnetodynamic Phenomena in the Solar Atmosphere - Prototypes of Stellar Magnetic Activity*, ed. Y. Uchida, T. Kosugi, & H. S. Hudson, 497

- Metcalf, T. R., Jiao, L., McClymont, A. N., Canfield, R. C., & Uitenbroek, H. 1995, *ApJ*, 439, 474
- Metcalf, T. R., et al. 2006, *Sol. Phys.*, 237, 267
- Mickey, D. L. 1985, *Sol. Phys.*, 97, 223
- Mickey, D. L., Canfield, R. C., Labonte, B. J., Leka, K. D., Waterson, M. F., & Weber, H. M. 1996, *Sol. Phys.*, 168, 229
- Molodensky, M. M. 1974, *Sol. Phys.*, 39, 393
- Parker, E. N. 1979, *Cosmical magnetic fields: Their origin and their activity* (Oxford, Clarendon Press; New York, Oxford University Press, 1979, 858 p.)
- Pevtsov, A. A., Balasubramaniam, K. S., & Rogers, J. W. 2003, *ApJ*, 595, 500
- Pevtsov, A. A., Canfield, R. C., & Latushko, S. M. 2001, *ApJ*, 549, L261
- Pevtsov, A. A., Canfield, R. C., & Metcalf, T. R. 1994, *ApJ*, 425, L117
- Pevtsov, A. A., Canfield, R. C., & Metcalf, T. R. 1995, *ApJ*, 440, L109
- Pevtsov, A. A., & Longcope, D. W. 2001, in *Astronomical Society of the Pacific Conference Series, Vol. 236, Advanced Solar Polarimetry – Theory, Observation, and Instrumentation*, ed. M. Sigwarth, 423
- Pevtsov, A. A., & Longcope, D. W. 2007, in *Astronomical Society of the Pacific Conference Series, Vol. 369, New Solar Physics with Solar-B Mission*, ed. K. Shibata, S. Nagata, & T. Sakurai, 99
- Povel, H. 1995, *Optical Engineering*, 34, 1870
- Rachkowsky, D. N. 1967, *Izv. Krymsk. Astrofiz. Obs.*, 37, 56

Richardson, R. S. 1941, *ApJ*, 93, 24

Rust, D. M. 1994, *Geophys. Res. Lett.*, 21, 241

Rust, D. M., & Kumar, A. 1996, *ApJ*, 464, L199

Sakurai, T., et al. 1995, *PASJ*, 47, 81

S'anchez Almeida, J. 1998, in *Astronomical Society of the Pacific Conference Series*, Vol. 155, *Three-Dimensional Structure of Solar Active Regions*, ed. C. E. Alissandrakis & B. Schmieder, 54

Sankarasubramanian, K., et al. 2004, in *Society of Photo-Optical Instrumentation Engineers (SPIE) Conference Series*, Vol. 5171, *Society of Photo-Optical Instrumentation Engineers (SPIE) Conference Series*, ed. S. Fineschi & M. A. Gummin, 207

Sankarasubramanian, K., et al. 2006, in *Astronomical Society of the Pacific Conference Series*, Vol. 358, *Astronomical Society of the Pacific Conference Series*, ed. R. Casini & B. W. Lites, 201

Schmidt, W., Beck, C., Kentischer, T., Elmore, D., & Lites, B. 2003, *Astronomische Nachrichten*, 324, 300

Seehafer, N. 1990, *Sol. Phys.*, 125, 219

Skumanich, A., & Lites, B. W. 1987, *ApJ*, 322, 473

Socas-Navarro, H. 2001, in *Astronomical Society of the Pacific Conference Series*, Vol. 236, *Advanced Solar Polarimetry – Theory, Observation, and Instrumentation*, ed. M. Sigwarth, 487

Solanki, S. K. 1989, *A&A*, 224, 225

- Staude, J., Hofmann, A., & Bachmann, G. 1991, in 11. National Solar Observatory / Sacramento Peak Summer Workshop: Solar polarimetry, p. 49 - 58, 49
- Stenflo, J. O. 1996, *Nature*, 382, 588
- Stenflo, J. O., & Keller, C. U. 1997, *A&A*, 321, 927
- Stepanov, V. E., & Severny, A. B. 1962, *Izv. Krymsk. Astrofiz. Obs.*, 28, 166
- Tiwari, S. K., Joshi, J., Gosain, S., & Venkatakrisnan, P. 2008, in *Turbulence, Dynamos, Accretion Disks, Pulsars and Collective Plasma Processes*, ed. S. S. Hasan, R. T. Gangadhara, & V. Krishan, 329
- Tsuneta, S., et al. 2008, *Sol. Phys.*, 249, 167
- Unno, W. 1956, *PASJ*, 8, 108
- Venkatakrisnan, P., & Gary, G. A. 1989, *Sol. Phys.*, 120, 235
- Wang, J., Shi, Z., Wang, H., & Lue, Y. 1996, *ApJ*, 456, 861
- West, E. A., & Hagyard, M. J. 1983, *Sol. Phys.*, 88, 51
- Wilkinson, L. K., Emslie, G. A., & Gary, G. A. 1989, *Sol. Phys.*, 119, 77